

Testing GRB models with the afterglow of GRB 090102

B. Gendre^{1*}, A. Klotz^{2,3}, E. Palazzi⁴, T. Krühler^{5,6}, S. Covino⁷, P. Afonso⁵,
L.A. Antonelli⁸, J.L. Atteia⁹, P. D’Avanzo⁷, M. Boër², J. Greiner⁵, and S. Klose¹⁰

¹Laboratoire d’Astrophysique de Marseille/Universit de Provence/CNRS, 38 rue Joliot curie, 13388 Marseille CEDEX 13, France

²Observatoire de Haute-Provence, F-04870 Saint Michel l’Observatoire, France

³CESR, Observatoire Midi-Pyrénées, CNRS, Université de Toulouse, BP 4346, F-31028 - Toulouse Cedex 04, France

⁴IASF-Bologna/INAF, via Gobetti 101, 40129, Bologna, Italy

⁵Max-Planck-Institut für extraterrestrische Physik, Giessenbachstrasse 1, 85748 Garching, Germany

⁶Universe Cluster, Technische Universität München, Boltzmannstrasse 2, 85748 Garching, Germany

⁷Osservatorio Astronomico di Brera/INAF, via Bianchi 46, 23807 Merate (LC), Italy

⁸Osservatorio Astronomico di Roma/INAF, via Frascati 33, 00040 Monteporzio Catone (RM), Italy

⁹LATT, Observatoire Midi-Pyrénées, CNRS, Université de Toulouse, 14 Avenue E. Belin, F-31400 - Toulouse, France

¹⁰Thüringer Landessternwarte Tautenburg, Sternwarte 5, 07778 Tautenburg, Germany

Accepted 2010 Feb 28. Received 2010 Feb 18; in original form 2009 Sept 07

ABSTRACT

We present the observations of the afterglow of gamma-ray burst GRB 090102. Optical data taken by the TAROT, REM, GROND, together with publicly available data from Palomar, IAC and NOT telescopes, and X-ray data taken by the XRT instrument on board the *Swift* spacecraft were used. This event features an unusual light curve. In X-rays, it presents a constant decrease with no hint of temporal break from 0.005 to 6 days after the burst. In the optical, the light curve presents a flattening after 1 ks. Before this break, the optical light curve is steeper than that of the X-ray. In the optical, no further break is observed up to 10 days after the burst. We failed to explain these observations in light of the standard fireball model. Several other models, including the cannonball model were investigated. The explanation of the broad band data by any model requires some fine tuning when taking into account both optical and X-ray bands.

Key words: gamma-ray: bursts

1 INTRODUCTION

Gamma-Ray Bursts (GRBs, see e.g. Piran 2005, for a review) were discovered in the late 1960’s (Klebesadel et al. 1973). For about three decades, their exact nature remained elusive. The effort to provide a fast re-pointing of the BeppoSAX satellite allowed for the first detection of their afterglows at all wavelengths (e.g. Costa et al. 1997; van Paradijs et al. 1997). Since then, the specification of each generation of instrumentation devoted to GRB studies included the need to point to the GRB afterglows quickly. Now, with *Swift*, we have reached the point where we can collect data from X-rays to optical within seconds after the start of the event, thanks to fast moving telescopes triggered by GCN notices (Barthelmy 1998). This run toward fast re-pointing has allowed for prompt optical emission ob-

servations by small autonomous telescopes for several GRBs (e.g. Klotz et al. 2009c).

Since the mid of the 1990’s, a theoretical canonical model has emerged in order to explain the GRB phenomenon: the fireball model (Rees & Mészáros 1992; Mészáros & Rees 1997; Panaitescu et al. 1998). This model is based on blast waves emitted by a progenitor during black hole formation, that interacts within a jet and/or with the surrounding medium to produce all observed emissions. These emissions are not thermal, and are proposed to be synchrotron emission from the electrons accelerated within the fireball. This model has the advantages that it is quite easy to apply and reproduces, reasonably well, the observations done by BeppoSAX and other telescopes (e.g. Gendre et al. 2006). The situation has, however, radically changed with the launch of the *Swift* satellite (Gehrels et al. 2004). *Swift* has discovered X-ray flares (O’Brien et al. 2006), an early flattening of the X-ray emission (Nousek et al. 2006), and several chromatic breaks within the afterglow light curves (e.g. Racusin et al. 2008), that were unexpected within the

* Present address : ASDC, Via Galileo Galilei, 00044 Frascati, Italy. E-mail:bruce.gendre@asdc.asi.it. Based on observations obtained with TAROT, REM, GROND.

initial standard model. This model has been modified in order to explain all these new features, including late energy injection (e.g. Ghisellini et al. 2007), multi-core or patchy jets (e.g. Peng et al. 2005, and references therein), and multi-component afterglow (e.g. Willingale et al. 2007). However, these modifications to the standard model were made only in order to explain a given feature, and sometimes lack a multi-wavelength consistency check. In previous years, several studies on peculiar events have led the realization that all available data could not be explained due to limitations within the standard model (e.g. Klotz et al. 2008).

In this article, we present observations of GRB 090102 at optical and X-ray wavelengths, taken over the 10 days following the burst. While the optical or X-ray data alone could be explained within the framework of the standard model, when combining these different datasets, the standard model alone cannot explain the observations of this burst, indicating that other models need to be tested. The paper is organized as follows: we present GRB 090102 in Sec. 2 with the data reduction and analysis in Sec. 3; we fit several models to these data in Sec. 4; finally, we discuss our findings in Sec. 5 before concluding. Errors on spectral and temporal indices (and the related closure relation values) are quoted at the 90% confidence level throughout. Reported errors on data points are 1σ errors.

2 GRB 090102

GRB 090102 triggered *Swift*-BAT (trigger 338895, Mangano et al. 2009a) on Jan. 2009, 2nd at 02:55:45 UT (hereafter, T_0). It was also recorded by Konus Wind (Golenetskii et al. 2009), and by INTEGRAL/SPI-ACS (Mangano et al. 2009b). The duration of this event, as observed by *Swift* was $T_{90} = 27.0 \pm 2.2$ s. Its light curve presents four peaks from $T_0 - 14$ s to $T_0 + 15$ s (Sakamoto et al. 2009). Its time averaged spectrum can be represented either using an exponential cutoff power law model or a Band model (Band et al. 1993), with parameters $\alpha = -0.86 \pm 0.14$, $\beta \leq -2.73$, and $E_p = 451_{-58}^{+73}$ keV ($\chi^2_\nu = 1.075$, 64 d.o.f.) and with a fluence of $3.09_{-0.25}^{+0.29} \times 10^{-5}$ erg cm⁻² (20 keV – 2 MeV, Golenetskii et al. 2009). Using the measured redshift ($z=1.547$, de Ugarte Postigo et al. 2009a), this gives $E_{\text{iso}} \sim 5.75 \times 10^{53}$ erg (1 keV – 10 MeV, rest frame) and a rest frame E_p of 1149_{-148}^{+186} keV, fully compatible with the so-called Amati relation (Amati et al. 2009, 2002).

Due to an observational constraint (Earth limb too close), *Swift* slewed to the position of the afterglow with a delay, and XRT and UVOT observations began only at $T_0 + 395$ s, observing a bright fading source in both the XRT and the UVOT fields of view (Mangano et al. 2009a). No optical observations were available during the prompt phase. The earliest ground search of the optical afterglow was performed by the Telescope a Action Rapide pour les Objets Transitoires (TAROT), starting at $T_0 + 40.8$ s (Klotz et al. 2009a). The Rapid Eye Mount (REM) robotic telescope also observed the field starting from $T_0 + 53$ s (Covino et al. 2009, note however that the start time reported in the GCN is not correct). A new source was detected at RA=08^h32^m58.52^s, Dec=+33°06′51.1″ (J2000.0)

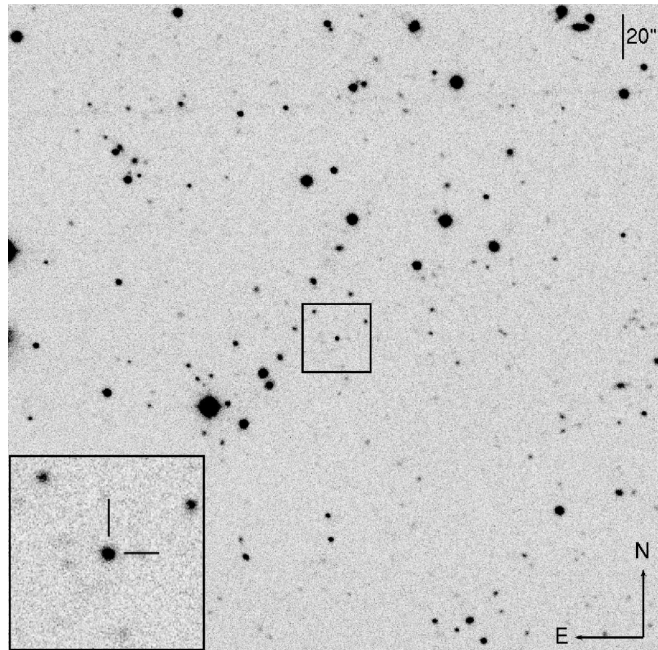


Figure 1. Image of the field of view of GRB 090102 from GROND, taken in the *i'* band 11 ks after the burst. The GRB afterglow is indicated by two ticks.

with an error of $0.3''$ (see Fig. 1). This source was then confirmed to be the optical afterglow of GRB 090102. Spectroscopic observations were carried by the Nordic Optical Telescope (NOT) (de Ugarte Postigo et al. 2009a), the Palomar 200" Hale telescope (Cenko et al. 2009), and by the Hobby-Eberly Telescope (Cucchiara & Fox 2009).

Late afterglow observations were performed by the Gamma-Ray burst Optical/Near-Infrared Detector (GROND) 2.50 h after the burst (Afonso et al. 2009), by the Instituto de Astrofísica de Canarias 80 cm telescope (IAC80) 19.2 h after the burst (de Ugarte Postigo et al. 2009b), and by the Palomar 60-inch telescope 50 min after the burst and later on (Cenko et al. 2009). The observations continued in the following days using the NOT (Malesani et al. 2009) and the HST (Levan et al. 2009), leading to the detection of the host galaxy.

A radio follow-up was also carried out using the VLA and the Westerbork Synthesis Radio Telescope (WSRT) at the 8.46 GHz (Chandra & Frail 2009) and the 4.9 GHz (van der Horst et al. 2009) wavelengths respectively. No afterglow was detected, leading to upper limits. Finally, the MAGIC Cerenkov Telescope also pointed to the position of the afterglow, without any detection (Gaug et al. 2009).

3 DATA REDUCTION AND ANALYSIS

3.1 X-ray data

The data were processed using the *ftools* version 6.6.2. To extract light curves and spectra, a rectangular box and circular extraction region were used for window timing and photon counting modes respectively, with an extraction region of 50 pixels in both cases. XRT observations began 395 seconds after T_0 in window timing mode. The instrument

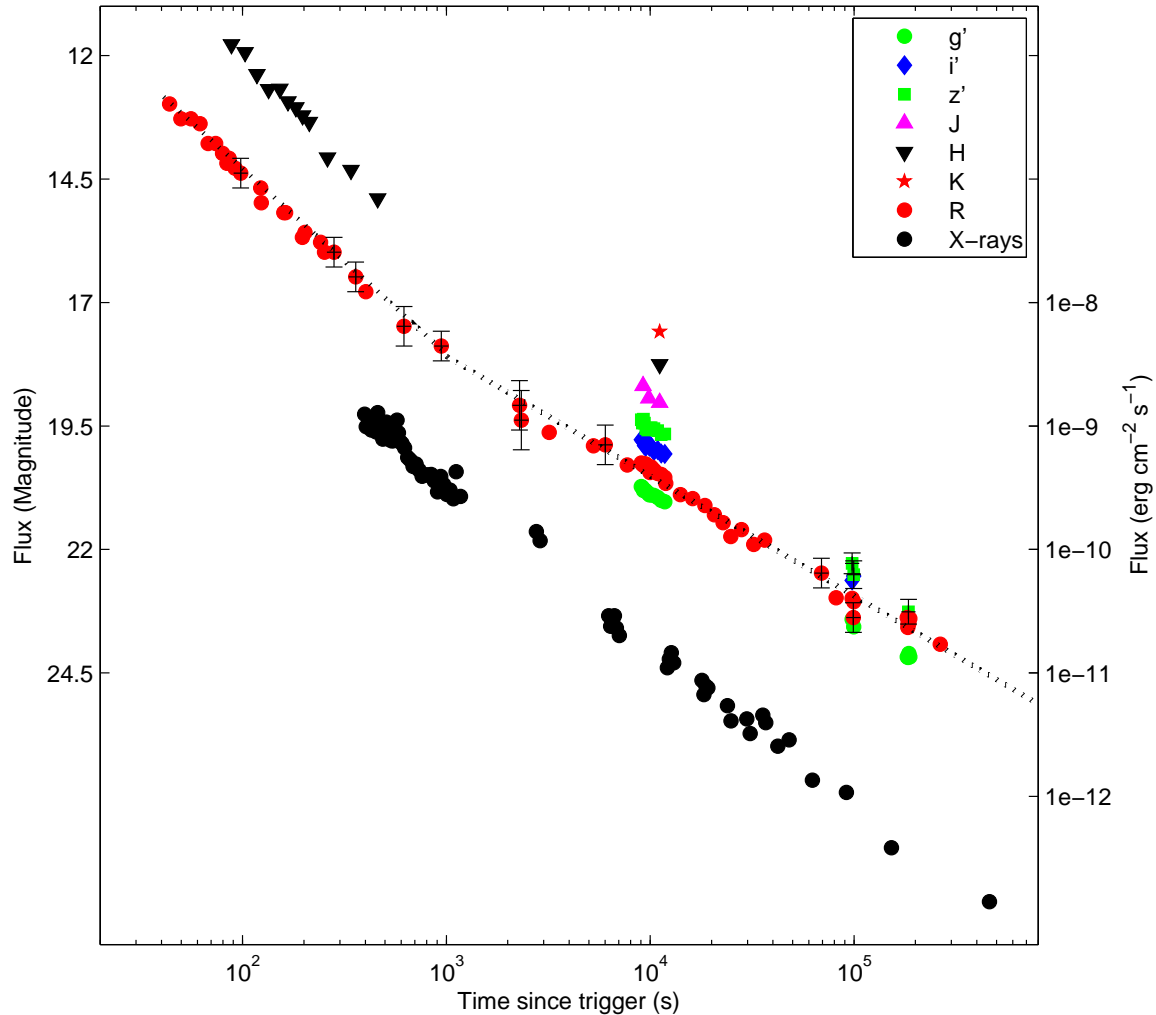


Figure 2. Light curve of the afterglow of GRB 090102 in X-ray, g', R, i', z', J, H, and K bands from Tables 1 and 2. For clarity, upper limits have been omitted. When not plotted, the error bars have the size of the symbols or smaller. These light curves have been corrected for the galactic extinction/absorption due to the Milky Way. The X-ray light curve is extracted in the 0.5 to 10.0 keV band. The dotted line is the best fit decay law (see text for details). The left axis applies to optical/infrared data, the right axis to X-ray data.

switched to the photon counting mode (see Hill et al. 2005) at $T_0 + 669.1$ s, while the count rate was high enough to cause pile up. As a matter of consequence, the observation between $T_0 + 669.1$ s and $\sim T_0 + 3000$ s suffers from severe to moderate pile up. This area was discarded in the following spectral analysis, and corrected within the light curve using the prescriptions of Vaughan et al. (2006).

All spectra were rebinned in order to include 20 net counts within each bin, and fit using the χ^2 statistic. The spectral model was composed of a power law continuum absorbed by our own galaxy ($N_H = 4.1 \times 10^{20} \text{ cm}^{-2}$, Dickey & Lockman 1990) and by the host galaxy at $z = 1.547$. Extracting spectra at several epoch, we did not find any evidence for spectral variation during the whole follow-up of the afterglow. The spectrum is well modeled ($\chi^2_\nu = 0.92$, 102 d.o.f.) by a single power law with spectral index

$\beta_X = 0.83 \pm 0.09$ absorbed in our own galaxy and by extragalactic absorbers ($N_H = 8.8^{+2.7}_{-2.5} \times 10^{21} \text{ cm}^{-2}$ when located within the host galaxy).

The light curve was extracted within the 0.5-10.0 keV band and rebinned in order to obtain at least 25 counts per bin. All decay index indicated below are derived from fits using the χ^2 statistic. We did not observe strong flares (see Fig. 2). A single moderate flare can be seen in the unbinned light curve during orbit 2 (corresponding to the period $\sim 2000 - 4000$ s after the trigger), which has been excluded from the temporal analysis. The complete light curve can be adequately fit ($\chi^2_\nu = 1.18$, 65 d.o.f.) using a single power law with a decay index $\alpha_X = 1.34 \pm 0.02$. A broken power law can also represent the data ($\chi^2_\nu = 0.99$, 63 d.o.f.) with $\alpha_{1,X} = 1.29 \pm 0.03$, $\alpha_{2,X} = 1.48 \pm 0.10$, and a break time $t_b = 18700^{+14500}_{-8000}$ s. With the observed steep-

ening, $\Delta\alpha = 0.19 \pm 0.11$, this break could be interpreted as the cooling frequency passing through the observation band. However, this should be associated with a spectral break not supported by the data. An F-test check on the break existence gives a probability of 0.26, i.e. a value not conclusive. One may note however that in this special case (large error on t_b that make it compatible with 0 within 3σ), the probability derived from the F-test should not be considered as valid (see Protassov et al. 2002). As a matter of consequence, in the following we will consider both hypotheses (single power law or broken power law), and report early and late X-ray data as data taken before and after the temporal break respectively.

3.2 Optical data

At the position of the afterglow, the Galactic extinction is $E(B - V) = 0.047$ according to Schlegel et al. (1998). We corrected all magnitudes using this estimation. Assuming $R_v=3.1$, this gives in particular $A_R=0.14$ (Pei 1992). The specific data processing relative to all instruments is indicated in the following subsections. We completed this sample by using reported observations by Cenko et al. (2009); de Ugarte Postigo et al. (2009b); Malesani et al. (2009). This extended sample of data taken in the R band is listed in Table 1.

3.2.1 TAROT data

We used data from TAROT Calern (Klotz et al. 2009d) that started an exposure of the field of GRB 090102 at $T_0+40.8$ s (duration 60 s) with the tracking speed adapted to obtain a small ten pixel trail. This technique was used in order to obtain continuous temporal information during the exposure (e.g. Klotz et al. 2006). The spatial sampling was $3.29''\text{pix}^{-1}$ and the FWHM of stars (in the perpendicular direction of the trail) was 2.05 pixels. Only the first exposure was performed with this technique. Successive images were tracked on the diurnal motion using exposure times increasing from 30 s to 180 s. Images are not filtered.

We used the star USNO-B1 1231-0206902 as a constant template for calibration during the trailed exposure. Contrary to the claim of Klotz et al. (2009a), TAROT did not observe a rise during the first part of the trailed image. Indeed, the profile is convolved by the Point Spread Function (PSF) that induces a slope at the start and at the end of the trail. The rapid analysis done by Klotz et al. (2009a) confused this slope with a rise at the start of the GRB afterglow trail. This has been corrected for by using the flux of the template (constant) star.

In order to precisely cross-calibrate the observations performed with REM and TAROT, we used several USNO stars as relative standards. All flux measurements were done using standard aperture photometry with the AuDela software¹. USNO-B1 1231-0206902 has been used to build the PSF in TAROT images in order to fit the flux of the GRB. TAROT observations are not filtered. We thus converted all TAROT instrumental magnitudes to standard R magnitudes, using the following formula: $R = C - 2.5 \times \log(F) +$

$(V - R) \times \alpha_r$. In this equation, $\alpha_r = 0.4$ is determined using calibration stars with various (V-R) values located within an open cluster. C is calculated for each image from the PSF flux, the R and (V-R) measurements of the reference stars.

3.2.2 REM data

Early time optical and NIR data were collected using the 60 cm robotic telescope REM (Zerbi et al. 2001; Covino et al. 2004) located at the ESO La Silla observatory (Chile). The telescope simultaneously feeds, by means of a dichroic, the two focal instruments: REMIR (Conconi et al. 2004) a NIR camera, operating in the range 1.0-2.3 μm (z', J, H and K), and ROSS (REM Optical Slitless Spectrograph, Tosti et al. 2004) an optical imager with spectroscopic (slitless) and photometric capabilities (V, R, I). Both cameras have a field of view of $10 \times 10'$.

REM reacted promptly and began observing 103 s after the GRB trigger time, following the event for ~ 1 hour (see Table 1). For the first 500 s REMIR observations were performed only in the H filter with increasing exposure times, then all the NIR filters were used in sequence. In the optical range only R band images were taken, for a total of 38 consecutive images. The transient was only detected up to 500 s both in the R and H bands, after which its luminosity falls below the instrument detection limits for all filters.

Each single NIR observation with REMIR was performed with a dithering sequence of five images shifted by a few arcseconds. These images are automatically elaborated using the proprietary routine AQuA (Testa et al. 2004). The script aligns the images and co-adds all the frames to obtain one average image for each sequence.

Each R image was reduced using standard procedures. A combination of the ESO-MIDAS² DAOPHOT task (Stetson 1988) and SExtractor³ package (Bertin & Arnouts 1996) was used to perform standard aperture photometry. The photometric calibration for the NIR was accomplished by applying average magnitude shifts computed using the 2MASS⁴ catalogue.

The optical data were calibrated using instrumental zero points and checked with observations of standard stars in the SA92 Landolt field (Landolt 1992). Results are displayed in Tables 1 and 2.

3.2.3 GROND data

The Gamma-Ray Burst Optical/NearInfrared Detector (GROND, Greiner et al. 2008) mounted at the 2.2 m ESO/MPI telescope at La Silla observatory imaged the field of GRB 090102 simultaneously in g'r'i'z'JHK starting 9.01 ks after T_0 under clear sky conditions (Afonso et al. 2009). At that point the location of the burst was becoming visible above the pointing horizon of the telescope. A total of 12 g'r'i'z' images with integration times of 66 s, 115 s and 375 s were obtained during the first night post burst. At the same time, NIR frames were acquired with a constant exposure of 10 s. In addition, the field was observed by GROND

² <http://www.eso.org/projects/esomidas/>

³ <http://astroa.physics.metu.edu.tr/MANUALS/sextractor/>

⁴ <http://www.ipac.caltech.edu/2mass/>

¹ <http://www.audela.org/>

Table 1. Table of data taken in the R band, corrected for galactic extinction. GROND data in r' band are transformed to Vega R system. Errors are given at 1σ level. Data from Palomar, IAC80 and NOT are taken from Cenko et al. (2009); de Ugarte Postigo et al. (2009b); Malesani et al. (2009) respectively.

Mid time (s)	Exposure duration (s)	Magnitude	Instrument	Mid time (s)	Exposure duration (s)	Magnitude	Instrument
43.8	6.0	13.0 ± 0.2	TAROT	9266	66	20.43 ± 0.03	GROND
49.8	6.0	13.3 ± 0.2	TAROT	9373	66	20.48 ± 0.06	GROND
55.8	6.0	13.3 ± 0.2	TAROT	9514	115	20.44 ± 0.04	GROND
61.8	6.0	13.4 ± 0.2	TAROT	9711	115	20.51 ± 0.02	GROND
67.8	6.0	13.8 ± 0.2	TAROT	9903	115	20.52 ± 0.02	GROND
73.8	6.0	13.8 ± 0.2	TAROT	9973.9	120	20.44 ± 0.07	Palomar
79.8	6.0	14.0 ± 0.2	TAROT	10091	115	20.50 ± 0.03	GROND
83.8	30	14.18 ± 0.10	ROSS	10423	375	20.56 ± 0.02	GROND
85.8	6.0	14.1 ± 0.2	TAROT	10868	375	20.63 ± 0.01	GROND
91.8	6.0	14.3 ± 0.2	TAROT	11320	375	20.65 ± 0.01	GROND
97.8	6.0	14.4 ± 0.3	TAROT	11780	375	20.71 ± 0.02	GROND
122.7	29.4	14.7 ± 0.1	TAROT	11911.5	120	20.66 ± 0.08	Palomar
123.6	30	14.98 ± 0.20	ROSS	14068.6	120	20.89 ± 0.09	Palomar
159.3	30.6	15.2 ± 0.2	TAROT	16144.7	120	20.97 ± 0.09	Palomar
162.4	30	15.18 ± 0.20	ROSS	18522.6	600	21.11 ± 0.06	Palomar
196.5	30.6	15.7 ± 0.2	TAROT	20631.5	600	21.30 ± 0.06	Palomar
202.2	30	15.58 ± 0.20	ROSS	22756.7	600	21.46 ± 0.07	Palomar
241.1	30	15.78 ± 0.20	ROSS	24832.6	600	21.74 ± 0.08	Palomar
252.3	67.8	16.0 ± 0.2	TAROT	27994.7	1200	21.60 ± 0.05	Palomar
280.8	30	15.98 ± 0.30	ROSS	32188.5	1200	21.90 ± 0.06	Palomar
358.6	90	16.48 ± 0.30	ROSS	36411.3	1200	21.81 ± 0.11	Palomar
402.3	185.4	16.8 ± 0.2	TAROT	69120.0	1800	22.48 ± 0.30	IAC80
619.5	330	17.48 ± 0.40	ROSS	81566	—	22.98 ± 0.20	NOT
943.8	685.2	17.9 ± 0.3	TAROT	97805	1500	23.16 ± 0.07	GROND
2283.0	2173.2	19.1 ± 0.5	TAROT	99200	—	23.38 ± 0.30	IAC80
2328.5	1380	19.38 ± 0.60	ROSS	99600	1500	23.23 ± 0.10	GROND
3190.2	120	19.63 ± 0.13	Palomar	182130	1500	23.55 ± 0.12	GROND
5266.2	120	19.90 ± 0.06	Palomar	183448	—	23.58 ± 0.20	NOT
6014.4	5275.2	19.9 ± 0.4	TAROT	183945	1500	23.67 ± 0.11	GROND
7704.3	120	20.29 ± 0.07	Palomar	185758	1500	23.67 ± 0.11	GROND
9042	66	20.42 ± 0.04	GROND	187575	1500	23.57 ± 0.09	GROND
9158	66	20.45 ± 0.03	GROND	264553	—	23.92 ± 0.09	NOT

at days 1 and 2 after the trigger. Data reduction was performed using standard IRAF tasks (Tody 1993), similar to the procedure outlined in Kruehler et al. (2008). Absolute photometry of the afterglow was measured relative to field stars from the SDSS and 2MASS catalogs, which yields average accuracies of 0.04 mag in g'r'i'z' and 0.07 mag in JHK, and are reported in Tables 1 and 2.

3.2.4 Temporal and spectral behaviors

The optical light curve can be fit using a broken power law model, with a break time on the order of 1000 s. As can be seen in Fig. 2, the light curve flattens at that time. It is worth noting that this flattening cannot be due to the host galaxy, fainter than $R \sim 24$ (Levan et al. 2009) when the afterglow magnitude is of the order of $R \sim 19 - 20$. Before the break, the decay index is $\alpha_{1,O} = 1.50 \pm 0.06$, steeper than the X-ray decay index at the same date (see Table 3). After the break, the decay index is $\alpha_{2,O} = 0.97 \pm 0.03$, flatter than the X-ray decay index at the same time. We do not observe any color variation (both in optical and in X-rays) before and after the temporal break seen in optical (see Table 4). If we assume the host extinction to be null, the value of $R - H =$

Table 3. Summary of the properties of GRB 090102.

Property	GRB 090102
Early optical decay index	1.50 ± 0.06
Late optical decay index	0.97 ± 0.03
X-ray decay index	1.34 ± 0.02
X-ray spectral index	0.83 ± 0.09

2.4 implies $\beta_{O,obs} = 1.32$. A non zero extinction would cause a flatter β_O , thus one should consider this as an upper limit: $\beta_O < 1.32$. The value of the optical-to-X-ray spectral index is $\beta_{OX} > 0.53 \pm 0.04$.

3.2.5 Optical extinction

The estimation of the optical extinction is a non-trivial problem, as we need to assume a spectral slope of the afterglow continuum in order to deduce the amount of extinction needed in the optical to reproduce that continuum (see e.g. Stratta et al. 2009). In this article we prefer to focus on the constraints we can set on the GRB models, and thus we cannot make any assumption on the afterglow continuum. As a

Table 2. Table of optical/infrared data taken in other bands. GROND data in g', i', z' bands are transformed to Vega system. All magnitudes are corrected for local extinction due to the Milky Way, and errors are given at 1σ .

Mid time (s)	Exposure duration (s)	Filter	Magnitude	Telescope	Mid time (s)	Exposure duration (s)	Filter	Magnitude	Telescope
9042	66	g'	20.73 ± 0.05	GROND	9266	66	z'	19.36 ± 0.05	GROND
9158	66	g'	20.75 ± 0.04	GROND	9373	66	z'	19.44 ± 0.08	GROND
9266	66	g'	20.81 ± 0.06	GROND	9514	115	z'	19.55 ± 0.10	GROND
9373	66	g'	20.80 ± 0.06	GROND	9711	115	z'	19.58 ± 0.06	GROND
9514	115	g'	20.82 ± 0.05	GROND	9903	115	z'	19.54 ± 0.05	GROND
9711	115	g'	20.86 ± 0.03	GROND	10091	115	z'	19.53 ± 0.04	GROND
9903	115	g'	20.90 ± 0.03	GROND	10423	375	z'	19.55 ± 0.04	GROND
10091	115	g'	20.90 ± 0.02	GROND	10868	375	z'	19.59 ± 0.04	GROND
10423	375	g'	20.91 ± 0.02	GROND	11320	375	z'	19.67 ± 0.02	GROND
10868	375	g'	20.95 ± 0.02	GROND	11780	375	z'	19.66 ± 0.05	GROND
11320	375	g'	21.01 ± 0.02	GROND	97805	1500	z'	22.28 ± 0.21	GROND
11780	375	g'	21.04 ± 0.02	GROND	99600	1500	z'	22.51 ± 0.28	GROND
97805	1500	g'	23.42 ± 0.08	GROND	184853	6000	z'	23.26 ± 0.25	GROND
99600	1500	g'	23.57 ± 0.10	GROND	9214	240	J	18.69 ± 0.07	GROND
182130	1500	g'	24.18 ± 0.20	GROND	9826	480	J	18.94 ± 0.05	GROND
183945	1500	g'	24.19 ± 0.15	GROND	11124	1200	J	19.03 ± 0.04	GROND
185758	1500	g'	24.11 ± 0.13	GROND	88.2	10.0	H	11.78 ± 0.05	REM
187575	1500	g'	24.18 ± 0.13	GROND	102.9	10.0	H	11.93 ± 0.03	REM
9042	66	i'	19.78 ± 0.06	GROND	117.6	10.0	H	12.38 ± 0.07	REM
9158	66	i'	19.81 ± 0.05	GROND	134.0	10.0	H	12.68 ± 0.04	REM
9266	66	i'	19.74 ± 0.04	GROND	152.1	10.0	H	12.67 ± 0.04	REM
9373	66	i'	19.90 ± 0.06	GROND	166.8	10.0	H	12.93 ± 0.03	REM
9514	115	i'	19.92 ± 0.05	GROND	182.4	10.0	H	13.05 ± 0.03	REM
9711	115	i'	19.84 ± 0.04	GROND	197.1	10.0	H	13.22 ± 0.07	REM
9903	115	i'	19.92 ± 0.04	GROND	212.6	10.0	H	13.35 ± 0.05	REM
10091	115	i'	19.92 ± 0.05	GROND	261.0	50.0	H	14.07 ± 0.07	REM
10423	375	i'	20.01 ± 0.03	GROND	340.5	50.0	H	14.32 ± 0.08	REM
10868	375	i'	19.99 ± 0.02	GROND	459.7	150.0	H	14.90 ± 0.06	REM
11320	375	i'	20.06 ± 0.02	GROND	9214	240	H	> 17.19	GROND
11780	375	i'	20.07 ± 0.02	GROND	9826	480	H	> 17.79	GROND
97805	1500	i'	22.63 ± 0.12	GROND	11124	1200	H	18.25 ± 0.07	GROND
99600	1500	i'	22.54 ± 0.12	GROND	9214	240	K _s	> 16.48	GROND
184853	6000	i'	23.44 ± 0.15	GROND	9826	480	K _s	> 17.18	GROND
9042	66	z'	19.37 ± 0.08	GROND	11124	1200	K _s	17.59 ± 0.07	GROND
9158	66	z'	19.44 ± 0.07	GROND					

Table 4. GRB 090102 afterglow R–H color. All magnitudes are corrected for local extinction due to the Milky Way.

Mid time (s)	R – H color
88.2	2.42 ± 0.25
102.9	2.47 ± 0.33
152.1	2.53 ± 0.24
166.8	2.25 ± 0.23
197.1	2.48 ± 0.27
11124	2.39 ± 0.08

matter of consequence, we have tried to fit the optical-near infrared SED without using the X-ray information, assuming a simple power-law model⁵. We have tested the most common models used, i.e. the Milky Way, the Large and Small

⁵ One should think that this is already an hypothesis on the data, i.e. that there is no spectral break located between the g' and the K bands.

Table 5. GRB 090102 optical SED fit result. We indicate for various models the best fit parameters and the goodness of the fit. Within the fit, the β_O parameter was not allowed to become negative. In all cases, the redshift was fixed to 1.547.

Model	A_v^{host}	β_O	χ_v^2	d.o.f.
Milky Way	0.35 ± 0.29	0.52 ^{+0.32} _{-0.36}	0.07	4
Large Magellanic Cloud	0.52 ^{+0.29} _{-0.38}	0.29 ^{+0.50} _{-0.28}	0.07	4
Small Magellanic Cloud	0.04 ^{+0.13} _{-0.04}	0.93 ^{+0.13} _{-0.22}	1.35	4
Calzetti law	0.77 ^{+0.23} _{-0.77}	0.1 ^{+1.0} _{-0.1}	1.19	4

Magellanic Clouds and the Calzetti law (see Calzetti et al. 1994; Stratta et al. 2004, and references therein). Results are reported in Table 5. As can be seen from that Table, all models are acceptable. However, the small value of χ_v^2 reported in some case indicates a statistical problem. In fact, the spectral index and the host extinction are degenerate parameters, as can be seen from Fig. 4: if the errors are defined in Table 5, this is only due to the fact that both A_v (for physical reason) and β_O (by hypothesis) are not allowed

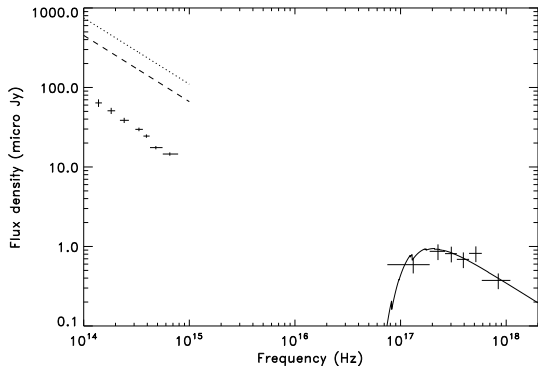


Figure 3. Spectral energy distribution of the afterglow of GRB 090102 observed 11.3 ks after the burst. Frequencies are expressed in the observer frame. The solid line represent the best fit X-ray model. Dotted line is the direct extrapolation of this model toward optical frequencies (assuming no extragalactic extinction). As there may be an X-ray flare at that time, we also rescaled this extrapolation (dashed line) to the level of the X-ray continuum at the same time.

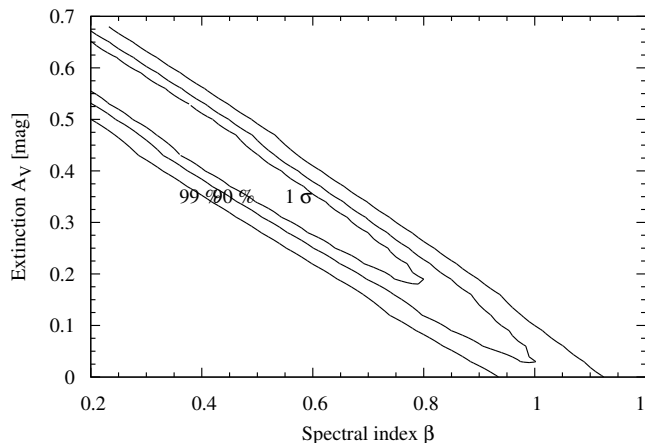


Figure 4. Contour plot in the β_O - A_V plane for a Large Magellanic Cloud extinction model. Contours are indicated for the 68%, 90% and 99% confidence levels. As one can see from the pronounced "banana-shape" of the plot, there is a strong degeneracy between these two parameters.

to become negative. As a matter of consequence, we cannot derive the host extinction from the optical photometric data alone.

However, we are able to provide two comments. First, in the host frame, we have an X-ray measurement of $N_H = 8.8^{+2.7}_{-2.5} \times 10^{21} \text{ cm}^{-2}$. This may imply that significant local extinction is present. Within our galaxy, this would lead to $A_V = 4.9^{+1.5}_{-1.4}$, that can be considered as an upper limit (see the discussion of Stratta et al. 2004).

Finally, in the host frame we have measurements ranging from 180.1 nm to 852.2 nm, i.e. covering the UV to \sim I bands. This last band should be the least affected by the host extinction. This is, however, not a band free of extinction,

and cannot be used to derive an estimation of the continuum flux density. Assuming that the optical and X-ray emissions are produced by the same mechanism, the true value is located between the data points and the dotted line on Fig. 3, corresponding to an extinction range of 0 – \sim 2.4 mag.

4 MODEL FITTING

4.1 Standard model

We first used the prescriptions of Panaitescu & Kumar (2000) and the X-ray data alone in order to test the standard model. They are summarized in Table 6 (from Sari et al. 1998; Sari & Piran 1999; Rhoads 1997). As one can see from this Table, in order to accommodate the standard model and the measurements made in X-ray, we should have the cooling frequency located above the X-ray band during the entirety of the observation. In such a case, a value of $p = 2\beta_X = 2.7 \pm 0.2$ can fit both the spectral and temporal X-ray indices if the surrounding medium has a constant density. However, a constant density medium implies that the cooling frequency is decreasing as $t^{-0.5}$. Any crossing of this frequency within the X-ray band would appear as a simultaneous increase in the spectral index by 0.5 and in the temporal decay index by 0.25. While the latter could be accommodated by the broken power law model, the former is not supported by the data. This implies that the cooling frequency should be above the X-ray band up to $\sim 5 \times 10^5$ s after the event, or above 800 keV at the start of the X-ray observation (thus implying very small values of ϵ_B and/or E_{tot} , the energy fraction located within the magnetic field and the total energy of the fireball respectively Panaitescu & Kumar 2000). This is unlikely; moreover, in such a case, according to the model, the optical light curve should decay either with the same slope than the X-ray light curve or with a decay index of 0.5 (Panaitescu & Kumar 2000): both hypotheses are ruled out by the data.

In conclusion, the standard model alone, in its simplest expression, cannot reproduce the global spectral and temporal behavior of the afterglow of GRB 090102.

4.2 Two component models

The afterglow of GRB 061126 features the same temporal and spectral behavior as the one of GRB 090102 (Perley et al. 2008; Gomboc et al. 2008, see also Table 3). These authors used a multi-component model rather than the standard fireball model in order to explain the broadband data of this burst. We thus checked if inserting an additional component to the fireball model could reproduce the data of the afterglow of GRB 090102.

The first step was to decide in which band we see the signature of the extra-component, and in which band the fireball model alone can reproduce both the spectral and temporal properties. In the standard fireball model, the fact that the optical and X-ray light curves do not present the same decay implies that a specific frequency (either the cooling or the injection frequency, see their definition in Mészáros 2006) is located between the optical and X-ray bands. Below the injection frequency, the decay index should be 0.5. With an optical decay of $\alpha_{1,O} = 1.50 \pm 0.06$, we can rule

Table 6. Closure relationships in the standard fireball model computed using the spectral and temporal information from the X-ray band. The specific frequency is ν_c (the cooling frequency) in the slow cooling regime, or ν_m (the injection frequency) in the case of fast cooling. All errors are quoted at the 90 % confidence level. Due to the absence of measured spectral index in the optical, optical values of the relationships are not reported

Medium class and geometry	Cooling regime	Specific frequency position	Closure relationship	Observed value		
				(single power law hypothesis)	X-rays (0.5-10.0 keV) (early broken power law)	(late broken power law)
Isotropic Wind	Fast	$\nu_m < \nu_X$	$\alpha - 1.5\beta + 0.5 = 0$	0.6 ± 0.2	0.5 ± 0.2	0.7 ± 0.3
		$\nu_m > \nu_X$	$\alpha - 0.5\beta = 0$	0.9 ± 0.1	0.9 ± 0.1	1.1 ± 0.2
	Slow	$\nu_c < \nu_X$	$\alpha - 1.5\beta + 0.5 = 0$	0.6 ± 0.2	0.5 ± 0.2	0.7 ± 0.3
		$\nu_c > \nu_X$	$\alpha - 1.5\beta - 0.5 = 0$	-0.4 ± 0.2	-0.5 ± 0.2	-0.3 ± 0.3
Isotropic ISM	Fast	$\nu_m < \nu_X$	$\alpha - 1.5\beta + 0.5 = 0$	0.6 ± 0.2	0.5 ± 0.2	0.7 ± 0.3
		$\nu_m > \nu_X$	$\alpha - 0.5\beta = 0$	0.9 ± 0.1	0.9 ± 0.1	1.1 ± 0.2
	Slow	$\nu_c < \nu_X$	$\alpha - 1.5\beta + 0.5 = 0$	0.6 ± 0.2	0.5 ± 0.2	0.7 ± 0.3
		$\nu_c > \nu_X$	$\alpha - 1.5\beta = 0$	0.1 ± 0.2	0.0 ± 0.2	0.2 ± 0.3
Jetted fireball	Slow	$\nu_c < \nu_X$	$\alpha - 2\beta = 0$	-0.3 ± 0.2	-0.4 ± 0.3	-0.2 ± 0.3
		$\nu_c > \nu_X$	$\alpha - 2\beta - 1.0 = 0$	-1.3 ± 0.2	-1.4 ± 0.3	-1.2 ± 0.3

out this hypothesis, and deduce that the cooling frequency needs to be located between the optical and X-ray bands. This is not compatible with the X-ray data (see Table 6): an extra component in the X-ray band is the only solution to solve this issue.

Under the above assumption, the optical band can be described by the fireball model and it is the X-ray band that needs an extra component in addition to the fireball in order to be described. This hypothesis needs to be confirmed by checking if the optical band can indeed be fit with the standard model. In fact, the flattening of the optical light curve around 1 ks is not possible in the standard model. However, several "common additions" to the standard model can provide an explanation: the addition of a reverse shock in the early optical data or a change in the surrounding medium density profile (the termination shock, see Chevalier et al. 2004; Ramirez-Ruiz et al. 2001). In the latter case, we can derive a value of $p = 4/3\alpha_{2,O} + 1 = 2.29 \pm 0.04$. The physical position of the termination shock cannot be constrained due to the presence of a second component in the X-ray data. We can thus conclude that our hypothesis is valid: the optical band can be fit with the standard model.

Lastly, one then needs to provide for the physical nature of the additional X-ray component. The requirements are that it needs to be: non-thermal, at all times brighter than the forward shock emission responsible for the optical emission, decaying monotonously without spectral variation, and producing few (if any) optical emissions. We do not conclude on the mechanism that produces these extra photons in X-ray. However, the latter requirement is the more constraining one, as already noted by Perley et al. (2008) for GRB 061126: it is quite difficult to accommodate a mechanism that produces X-rays without also producing optical photons. Note additionally that late in the light curve (after 1 ks), the standard model implies that the X-ray spectral index is $p/2 \sim 1.2$. The additional component needs to produce hard photons in order to obtain $\beta_X = 0.83 \pm 0.09$.

4.3 The cannonball model

In the cannonball model, GRBs and their afterglows are produced by bipolar jets of highly relativistic plasmoids (CB) of ordinary matter ejected in the birth of neutron stars or black holes (see e.g. Dado et al. 2009, and references therein).

A prompt, hard X-ray/gamma-ray pulse is produced by the thermal electrons in the CB plasma, via inverse Compton scattering of photons emitted/scattered into a cavity created by the wind/ejecta blown from the progenitor star or a companion star long before the GRB itself. Slightly later, when the CB encounters the wind/ejecta, the electrons of the ionized gas in front of it are swept into the CB and are Fermi accelerated by its turbulent magnetic field, emitting synchrotron radiation that dominates the prompt optical emission and the broad band afterglow emission. Thus, the observed emissions are due to two components: a short lasting Inverse Compton Scattering component, seen only at high energy, and a classical synchrotron emission (Dado & Dar 2009).

Following the notations and prescriptions of Dado et al. (2009), we can explain all the X-ray data assuming that we observe the synchrotron emission of a CB traveling within a medium of constant density (the so-called ISM) with the bend frequency located below the X-ray band. From the model, which gives, in that case $\beta_X = p/2$, we can derive $p = 1.7 \pm 0.2$. This value of p implies $\alpha_X = \beta + 0.5 = p/2 + 0.5 = 1.35 \pm 0.1$, in perfect agreement with our finding ($\alpha_X = 1.34 \pm 0.02$). We note that this value of p is lower than 2, and thus there should be a break/cutoff located at high energy so that the electron energy remains finite.

In the optical, things are more complicated. According to Dado et al. (2009), the spectral index in the optical should evolve from $\beta_O \approx 0.5$ during the prompt emission to $\beta_O \approx 0.83 \pm 0.09$ (i.e. the same as that in X-ray) during the late-time afterglow. Both values are compatible with the constraint derived from the color of the afterglow ($\beta \leq 1.32$). During the prompt optical emission, the decay index should be $\alpha_O = \beta_O + 1 \approx 1.5$ (see Eq. 33 in Dado et al. 2009). This is consistent with the observed value of $\alpha_{1,O} = 1.50 \pm 0.06$. The flattening of the optical light curve may be explained by a transition from a wind envi-

ronment to an ISM (as in the fireball model, see above). In such a case, the light curve should reach an asymptotic decay with $\alpha_{2,O} = \alpha_X = 1.34 \pm 0.09$ (see Eqs. 29 and 30 in Dado et al. 2009). We observed a value of $\alpha_{2,O} = 0.97 \pm 0.03$. However, the value of $\alpha_{2,O} = 1.34 \pm 0.09$ is only an asymptotic value, and the observed could vary if the observation is close to the time of the crossing of the bend frequency. In fact, we should observe an effective temporal decay index $\alpha_2(t) = \beta_O(t) + 1/2$ evolving from $\alpha_2 \sim 1$ to $\alpha_2 = 1.34 \pm 0.02$. Being close to the asymptotic value, the measurement is marginally compatible with the CB model expectation. Lack of late time temporal and spectral data prevents a confirmation of this prediction. Indeed, once reaching the asymptotic values, the CB model indicates that we should observe the same spectral and temporal behavior for the optical and X-ray bands. Looking to Fig. 3, this is hardly supported by the data. However, a large gray extinction, with $A_I \sim 2.5$ would make compatible the optical and X-ray emissions. In the absence of information about the host extinction, we cannot rule out such an extinction, and the CB model may indeed reproduce all the data with the expense of a few fine tunings.

5 DISCUSSION AND CONCLUSIONS

We have presented observations of the afterglow of GRB 090102. We used data taken by optical telescopes and by the XRT on board the *Swift* spacecraft. The light curve of this event features an unusual behavior. In X-rays, it presents a very smooth light curve with no hint of a temporal break. In the optical, the light curve presents a steep-flat behavior, with a break time at ~ 1 ks after the burst. This unusual light curve was also observed with GRB 061126. The standard fireball model cannot reproduce the observations without the addition of several components. The addition of a component at high energy solves the discrepancies between the optical and X-ray emissions. The optical data could then be interpreted as either due to a termination shock, locating the end of the free-wind bubble at the position of the optical break; or as a normal fireball expanding in an ISM, with a reverse shock present at an early time (less than 1 ks after the event). Any radio observations that could constrain the ISM density value would also constrain the wind density, and thus a key property of the progenitor of this GRB. However, the weak point of this model is that requires strong fine tuning in order to suppress the optical emission of the additional component, responsible for the X-ray emission. The cannonball model can also partly reproduce the data. It appears clear, however, that in order to explain the broadband emission, some fine-tuning of this model is mandatory, likewise for the fireball model.

The strange behavior of GRB 090102 provides a useful test-event for models that attempt to reproduce and explain the GRB phenomenon. The choice of the models tested here was strongly limited by the very small number of models that have published formulae of the temporal and spectral indices for GRB afterglows. Of course, we do not pretend to be exhaustive in our testing as the array of alternative models is huge. *Swift* has shown the diversity of GRB afterglows, and it may now be time for observers to test and reduce the diversity of GRB afterglow models.

ACKNOWLEDGMENTS

The authors thank G. Stratta for help during X-ray data analysis, and A. Dar for his kind and valuable help during the cannonball model analysis. Thanks are also due to K. Dzurella for help during the language improvement of the paper. B. Gendre acknowledges support from *Centre National d'Etudes Spatiales* (CNES). TK acknowledges support by the DFG cluster of excellence 'Origin and Structure of the Universe'.

REFERENCES

- Afonso, P., Krühler, T., Klose, S., & Greiner, J., 2009, GCN # 8771
- Amati, L., Frontera, F., Tavani, M., et al., 2002, A&A, 390, 81
- Amati, L., Guidorzi, C., Frontera, F., et al., 2009, MNRAS, 391, 577
- Band, D., Matteson, J., Ford, L., et al., 1993, ApJ 413, 281
- Barthelmy, S., 1998, in AIP Conf. Proc. 428, Gamma-Ray bursts, ed. C. Meegan & R. Preece (Berlin: Springer), 99
- Bertin, E., & Arnouts, S. 1996, A&AS, 117, 393
- Calzetti, D., Kinney, A.L., & Storchi-Bergmann, T., 1994, ApJ, 429, 582
- Lenz, S.B., Rau, A., & Salvato, M., 2009, GCN # 8773
- Chandra, P., & Frail, D.A., 2009, GCN # 8779
- Chevalier, R.A., Li, Z.Y., & Fransson, C., 2004, ApJ, 666, 369
- Conconi, P., Cunniffe, R., DAlessio, F., et al. 2004, Proc. SPIE, 5492, 1602
- Costa, E., Frontera, F., Heise, J., et al., 1997, Nature, 387, 783
- Covino, S., Stefanon, M., Fernandez-Soto, A., et al. 2004, SPIE, 5492, 1613
- Covino, S., D'Avanzo, P., Antonelli, L.A., et al., 2009, GCN # 8763
- Cucchiara, A., & Fox, D., 2009, GCN # 8774
- Dado, S., Dar, A., & De Rújula, A., 2009, ApJ 696, 994
- Dado, S., & Dar, A., 2009, astro-ph/0910.0687
- Dickey, J.M., & Lockman, F.J., 1990, ARAA 28, 215
- Gaug, M., Covino, S., Garczarezyk, M., et al., 2009, Contribution to the 31st ICRC, Lodz, Poland, July 2009, astro-ph:0907.0996
- Gehrels, N., Chincarini, G., Giommi, P., et al., 2004, ApJ, 611, 1005
- Gendre, B., Corsi, A., & Piro, L., 2005, A&A, 455, 803
- Ghisellini, G., Ghirlanda, G., Nava, L., & Firmani, C., 2007, ApJ, 658, L75
- Golenetskii, S., Aptekar, R., Mazets, E., et al., 2009, GCN # 8776
- Gomboc, A., Kobayashi, S., Guidorzi, C., et al., 2008, ApJ, 687, 443
- Greiner, J., Bornemann, W., Clemens, C., et al. 2008, PASP, 120, 405
- Hill, J.E., Angelini, L., Morris, D.C., et al., 2005, SPIE, 5898, 325
- Klebesadel, R., Strong, I., & Olson, R., 1973, ApJ 182, L85
- Klotz, A., Gendre, B., Stratta, G., et al., 2006, A&A, 451, L39
- Klotz, A., Gendre, B., Stratta, G., et al., 2008, A&A, 483, 847

- Klotz, A., Gendre, B., Boër, M., & Atteia, J.L., 2009a, GCN # 8761
- Klotz, A., Gendre, B., Boër, M., & Atteia, J.L., 2009b, GCN # 8764
- Klotz, A., Boër, M., Atteia, J.L., & Gendre, B., 2009c, AJ 137, 4100
- Klotz, A., Boër, M., Eysseric, J., 2009d, PASP 120, 1298
- Kruehler, T., Küpcü, Y.A., Greiner, J., et al. 2008, ApJ, 685, 376
- Landolt, A. U. 1992, AJ, 104, 340
- Levan, A.J., Malesani, D., Tanvir, N.R., et al., 2009, GCN # 8856
- Mangano, V., Barthelmy, S.D., Burrows, D.N., et al., 2009a, GCN # 8762
- Mangano, V., Markwardt, C.B., Barthelmy, S.D., et al., 2009b, GCN Report 192.1
- Malesani, D., Fynbo, J.P.U., de Ugarte Postigo, A., et al., 2009, GCN # 8780
- Mészáros, P., & Rees, M.J., 1997, ApJ, 476, 232
- Mészáros, P., 2006, Reports on Progress in Physics, 69, 2259
- Nousek, J. A., Kouveliotou, C., Grupe, D., et al., 2006, ApJ, 642, 389
- O'Brien, P. T., Willingale, R., Osborne, J., et al., 2006, ApJ, 647, 1213
- Panaitescu, A., Mészáros, P., & Rees, M.J., 1998, ApJ, 503, 314
- Panaitescu, A., & Kumar, P., 2000, ApJ 543, 66
- Pei, Y.C., 1992, ApJ, 395, 130
- Peng, F., Königl, A., & Granot, J., 2005, ApJ 626, 152
- Perley, D.A., Bloom, J.S., Butler, N.R., et al., 2008, ApJ 672, 449
- Protassov, R., van Dyk, D.A., Connors, A., Kashyap, V.L., & Siemiginowska, A., 2002, ApJ, 571, 545
- Racusin, J.L., Karpov, S.V., Sokolowski, M., et al., 2008, Nature 455, 183
- Sakamoto, T., Barthelmy, S.D., Baumgartner, W.H., et al., 2009, GCN # 8769
- Piran, T., 2005, RvMP, 76, 1143
- Ramirez-Ruiz, E., Dray, L.M., Madau, P., Tout, C.A., 2001, MNRAS, 327, 829
- Rees, M.J., & Mészáros, P., 1992, MNRAS, 258, 41
- Rhoads, J.E., 1997, ApJ, 487, L1
- Sari, R., Piran, T. & Narayan, R. 1998, ApJ, 497, L17
- Sari, R. & Piran, T. 1999, ApJ, 520, 641
- Schlegel, D.J., Finkbeiner, D.P., & Davis, M., 1998, ApJ 500, 525
- Stetson, P. B. 1988, PASP, 99, 191
- Stratta, G., Fiore, F., Antonelli, A., et al., 2004, ApJ, 608, 846
- Stratta, G., Pozanenko, A., Atteia, J.L., et al., 2009, A&A, 503, 783
- Testa, V., Antonelli, A., Di Paola, A., et al., 2004, SPIE 5496, 729
- Tody, D. 1993, in ASPC Ser., Vol. 52, Astronomical Data Analysis Software and Systems II, 173
- Tosti, G., Bagaglia, M., Campeggi, C., et al. 2004, Proc. SPIE, 5492, 689
- de Ugarte Postigo, A., Jakobsson, P., Malesani, D., et al., 2009a, GCN # 8766
- de Ugarte Postigo, A., Blanco, L., & Castro-Tirade, A.J., 2009b, GCN # 8772
- van der Horst, A.J., Wijers, R.A.M.J., & Kamble, A.P., 2009, GCN # 8792
- van Paradijs, J., et al., 1997, Nature, 386, 686
- Vaughan, S., Goad, M.R., Beardmore, A.P., et al., 2006, ApJ 638, 920
- Willingale, R., O'Brien, P. T., Osborne, J. P., et al., 2007, ApJ, 662, 1093
- Zerbi, F. M., Chincarini, G., Ghisellini, G., et al. 2001, Astron. Nach., 322, 275